# Amplifying Fibre Optic Sensor Signals with Graphene Oxide-Silver Nanostars

*Azib Haiman Roslan, Siti Rabizah Makhsin[*], Rozina Abdul Rani*
*School of Mechanical Engineering, College of Engineering, Universiti Teknologi MARA, 40450 Shah Alam, Selangor, MALAYSIA*
*[*]sitirabizah@uitm.edu.my*

*Beenish Siddique*
*AEH Innovative Hydrogel Ltd, Graphene Engineering Innovation Centre, Sackville St, Manchester M1 3BB, UNITED KINGDOM*

ABSTRACT

*This work presents a straightforward yet impactful method to enhance optical fibre sensor signals by integrating silver nanostars (AgNS) with graphene oxide (GO-AgNS) as a sensing material. AgNS were synthesized successfully via a one-step chemical reduction method using hydroxylamine as a reducing agent. The concentration of hydroxylamine was varied (7.2, 3.6, 1.8, and 0.9) x $10^{-4}$ %v/v to optimize AgNS formation, with the longest spike of the nanostar observed at lower hydroxylamine concentrations, as confirmed by transmission electron microscopy (TEM). UV-visible measurements revealed the highest peak absorption for AgNS synthesized using 0.9 x $10^{-4}$ %v/v hydroxylamine, 0.05 M sodium hydroxide, 0.8 mM silver nitrate, and 0.045 M sodium citrate, with an average length of 352.62 ± 59.72 nm measured from TEM images. GO was synthesized via a modified Hummer's method and mixed with AgNS at varying ratios (1:5, 1:10, 1:15, and 1:20) to form GO-AgNS coatings for the fibre optic probe. The GO-AgNS coating at a ratio of 1:5 exhibited the highest light absorption intensity, enhancing optical signal by 218% compared to GO-coated and 174% compared to AgNS-coated fibre optic sensors. These findings demonstrate that embedding AgNS onto the GO matrix structure as a sensing material significantly improves sensor performance, suggesting promising applications for super-sensitive, cost-effective, and rapid detection in fibre optic-based sensors.*

**Keywords:** *Fibre Optic Sensor; Graphene Oxide; Modified Hummer's Method; Silver Nanostar; Optical Signal Enhancement*

ISSN 1823-5514, eISSN 2550-164X

https://doi.org/10.24191/jmeche.v21i3.27359

Received for review: 2024-03-19
Accepted for publication: 2024-06-04
Published: 2024-09-15

## Introduction

Fibre optics find extensive use across various sectors including telecommunications, mechanical inspections, communications, and medical biosensor detection [1]. Fibre optics is made up of glass or silicon rods where the light passes through the rod over long distances with minimal loss [2]. These fibre optics are famous for their lightweight, sturdiness, and sensitiveness in light, making them suitable to be applied in small and tight spaces. When light encounters the surface of the core fibre, total internal reflection (TIF) occurs within the medium as the light hits the surface at angles exceeding the critical angle [3]. Through repeated occurrences of TIF, an evanescent field is generated outside the medium, producing evanescent waves as light traverses along [4]. In sensing applications, these waves serve as sensors by detecting changes in light sensitivity, refractive index, biology detections, and gas detection [5]. Consequently, various methods have been explored to enhance the optical performance of fibre optics. Among these methods, the recent application of noble metal nanoparticles to fibre optics has gained attention due to the unique capabilities of these nanoparticles as enhancers for optical sensors.

Advancements in nanotechnology have facilitated the production of thinner material layers in optical fibre, resulting in improved sensitivity, range, and accuracy [6]. Nanotechnology such as carbon nanotubes [7], polymeric nanocomposite [8], and plasmonic nanomaterials [9] has been applied to fibre to enhance its optical properties. Among these nanotechnology, plasmonic nanomaterial shows promising properties in sensing applications due to its sensitivity to light and its ability to manipulate the light at the nanoscale [10]. Plasmonic nanomaterial uses metallic nanostructures or noble metal nanoparticles (NMNPs) to enhance the localised surface plasmonic resonance (LSPR) when excited by the incident light or TIF in the fibre. LSPR occurs when the free electrons on the surface of the metal nanoparticles collectively oscillate in response to the incident electromagnetic field [11]. This resonance leads to strong absorption and scattering of light at specific wavelengths, which can be precisely tuned by adjusting the nanoparticles' size, shape, and composition. Thus, using the SPR effect in NMNPs in sensors should enhance the optical properties and signal of the embedded fibre.

Multiple studies have been reported where plasmonic nanomaterials such as silver nanoparticles (AgNPs) and gold nanoparticles (AuNPs) can significantly change physical, biological, and chemical properties due to their unique surface-to-volume ratio. Consequently, these nanoparticles have been employed for various purposes, notably in aiding graphene in enhancing biosensor applications [12]. Moreover, by applying these noble metals to fibre optics, the nanomaterial can exhibit strong LSPR properties which can be used to detect proteins, and bacteria when fibre optics is in contact with organic substances. AgNPs show exceptional sensitivity in sensor applications than

AuNPs [13] despite their lack of stability compared to AuNPs. For instance, when comparing the performance of AuNPs versus AgNPs used as coatings with the electrochemical marker for oligonucleotide sensors, both yield identical sensitivity and selectivity [14]. However, AgNPs demonstrate superior suitability for detecting DNA sensors compared to AuNPs. Additionally, AgNPs are more cost-effective to synthesize [13], making them more suitable for mass-producing highly sensitive DNA sensors. Moreover, AgNPs come in different shapes and each shape has its distinct properties and characteristics. Several techniques including top-down and bottom-up methods [15] in synthesizing AgNS have been used to create various shapes and sizes such as nanosphere, nanowire, nanocube, and more [16]. The nanostar-shaped silver nanostars (AgNS) represent compelling nanostructures with robust plasmonic properties, exhibiting notably lower plasmonic losses compared to other shapes in the UV-visible spectrum [17]. This characteristic primes AgNS to effectively enhance sensor signals, particularly in plasmonic biosensing applications [12]. In the realm of fibre optic sensors, optimizing the sensitivity hinges on augmenting both the evanescent wave and SPR, thus AgNPs emerge as highly suitable nanomaterials for attaining these objectives [4].

Nevertheless, the inherent instability of AgNS mandates the utilization of a stabilizing agent to enhance its longevity. Among the available options, graphene oxide (GO) emerges as the optimal choice [18]. The hexagonal structure of graphitic provides an ideal platform for embedding AgNS, effectively bolstering its stability and mitigating agglomeration. Additionally, recent studies [19] have highlighted GO's remarkable biocompatibility and expansive surface area, facilitating enhanced immobilization of biorecognition elements, and thereby amplifying biomolecule detection sensitivity, rendering it well-suited for biomedical sensor applications. The widely adopted method for synthesizing GO is the modified Hummers' method [20], renowned for its safety and scalability. This method involves the exfoliation of graphite, breaking it down into multiple layers, followed by oxidation. During oxidation, oxygen compounds combine with a few layers to form a single-layer GO structure, resulting in a graphene oxide layer with a graphitic structure.

A previous study demonstrated that incorporating spherical-shaped silver nanoparticles (AgNPs) with graphene oxide (GO) effectively mitigated AgNPs agglomeration, enhancing their antibacterial properties due to GO's exceptional characteristics [21]. Leveraging GO's remarkable structural properties, AgNPs-GO composites exhibit promising attributes such as enhanced optical sensitivity for heavy metal ion tracing, increased adsorption affinity, and catalytic activity in organic compound removal. However, the key challenge lies in ensuring the stability of Ag, especially in star shape (AgNS) and preventing agglomeration before embedding them with GO to maximize their effectiveness within the GO matrix. Therefore, utilizing AgNS, known for their superior stability compared to spherical AgNPs, in combination with

GO, is expected to further enhance plasmonic performance, thereby improving the sensing capabilities of fibre optics embedded with AgNS.

The primary aim of this study is to assess the effectiveness of a novel composite material, AgNS-GO, in augmenting the signal of fibre optic sensors compared to utilizing individual sensing elements (AgNS or GO). AgNS synthesis is accomplished through a one-step chemical reduction method employing hydroxylamine as the reducing agent. By varying the reducing agent concentration, we aim to explore the resulting morphological structure, particularly the formation of the star shape, and its correlation with optical properties. The most promising AgNS samples, demonstrating favourable optical and morphological attributes, are then combined with GO at different volume ratios (1:5, 1:10, 1:15, and 1:20). Characterization techniques utilized include scanning electron microscopy (SEM)/field emission SEM (FESEM), transmission electron microscopy (TEM), energy dispersive X-ray (EDX) spectroscopy, and UV-Vis spectroscopy, offering insights into morphological structure, elemental composition, and optical properties. The findings will illuminate the stability of AgNS and their potential for enhancing optical signal sensing capabilities. Furthermore, understanding the coating behaviour of the composite sensing materials (GO-AgNS) versus individual elements (GO or AgNS) on the fibre-optic sensing platform will be pivotal in determining overall sensor performance.

## Materials and Methods

### Materials

The chemicals required in synthesizing AgNS were silver nitrate; $AgNO_3$ (≥99.8%, Merck), sodium hydroxide; NaOH (99%, Merck), sodium citrate tribasic dihydrate; $Na_3C_6H_5O_7$ (≥99, Sigma-Aldrich), and hydroxylamine; $H_3NO$ (50 wt.% in $H_2O$, Sigma-Aldrich). The chemicals required in synthesizing GO were graphite powder; C (<20 µm, Sigma), sulphuric acid; $H_2SO_4$ (98%, Supelco), potassium permanganate; $KMnO_4$ (≥99%, R&M), hydrogen peroxide; $H_20_2$ (30%, Sigma-Aldrich), hydrochloric acid; HCl (37%, Supelco).

### Synthesis of Silver Nanostars (AgNS)

In our previous work [22], a stable of AgNS was successfully synthesized using a chemical reduction method with 9 mL of 1 x $10^{-3}$ M of silver nitrate ($AgNO_3$), 0.5 mL of 1.8 x $10^{-4}$ % v/v of hydroxylamine, 0.5 mL of 0.05 M of sodium hydroxide (NaOH) and 0.1 mL of 0.045 M of sodium citrate tribasic dehydrate found to be the optimum synthesis conditions. In this study, various concentrations of hydroxylamine were investigated to enhance the elongation of AgNS spikes, as detailed in Table 1. Similar steps were taken as previously

reported [22] to synthesize AgNS samples (sample ID: L, M, N, O) with longer spikes.

Table 1: AgNS parameters with different hydroxylamine concentrations

| Sample ID | NaOH (M) | Hydroxylamine (% v/v) | $AgNO_3$ (M) | Sodium citrate (M) |
|---|---|---|---|---|
| L | 0.05 | $7.2 \times 10^{-4}$ | $8 \times 10^{-4}$ | 0.045 |
| M | | $3.6 \times 10^{-4}$ | | |
| N | | $1.8 \times 10^{-4}$ | | |
| O | | $0.9 \times 10^{-4}$ | | |

## Synthesis of Graphene Oxide (GO)

The GO was synthesized via a modified Hummer method with a slight modification of previous work [18]. Here, 1 g of graphite powder was mixed with 25 mL of sulphuric acid under vigorous stirring at 600 rpm for 5 mins with an ice bath setting. Then, 3 g of potassium permanganate was added slowly to the black mixture solution and continued stirring for 3 hours while maintaining the temperature below 20 °C at the same stirring condition. The solution changed from black to green when adding potassium permanganate. If the solution turns pink instead of green, it indicates the exfoliation process has failed and the procedure needs to redo again. The ice bath was then removed, and 50 mL of distilled water was added dropwise into the solution while maintaining the temperature below 50 °C to undergo the oxidation process. After 5 minutes, the colour solution changes into dark brown indicating the formation of GO. Later, 100 mL of distilled water was added to complete the oxidation process followed by the addition of 5 mL of hydrogen peroxide to stop the reaction. The solution obtained was then cooled at room temperature and left overnight to separate the supernatant and precipitate (GO).

On the following day, the supernatant was removed, and the GO underwent multiple cycles of washing via centrifugation at 6000 rpm for 20 minutes with a solution of 5% v/v hydrochloric acid, followed by rinsing with distilled water. The thoroughly washed GO was then collected and deemed ready for use.

## Synthesis of Graphene Oxide-Silver Nanostars (GO-AgNS)

The GO solution obtained in the previous step was sonicated at 50 °C for 30 minutes to disperse the GO into smaller particles and prevent agglomeration. Subsequently, one part of this GO solution was mixed with 5 parts of AgNS and vortexed at 2000 rpm for 30 minutes. This process was repeated to prepare the GO-AgNS samples at ratios of 1:10, 1:15, and 1:20.

## Fabrication of fibre optics embedded with GO-AgNS

The sensing platform of fibre optic sensors was prepared by removing the protective layers of fibre optics cable (single mode of FC-FC type) via mechanical etching. The process began by manually unclad the sheathing, jacket, and cladding using a fibre optics stripper leaving only core fibre optics with a length of 2 cm as in Figure 1(a). The core fibre optics were then cleaned with ethanol to remove dust and small particles on the core surface. The unclad probes were then ready to be coated with GO, AgNS, and GO-AgNS samples via a dipping process. The dipping process began by dipping the core fibre optics with sensing material (AgNS, GO, or GO-AgNS with the ratio of 1:5, 1:10, 1:15 and 1:20) for 24 hours before drying them at room temperature for 12 hours.

Next, the core end of coated fibre optics was cleaved using FC-8R Precision Automatic Blade Rotation Fibre Cleaver (Sumitomo, USA) to ensure the end core of fibre optics was cleanly cut. Both ends of the core of fibre optics were then spliced together using Sumitomo Type-39 FastCat Core Alignment Fusion Splicer Kit 1 (see Figure 1(b)) to secure the connection of the core with another cable probe which completes the circuit for the detection. The splices of coated fibre optics were ready to be tested using a sensor setup as shown in Figure 2.

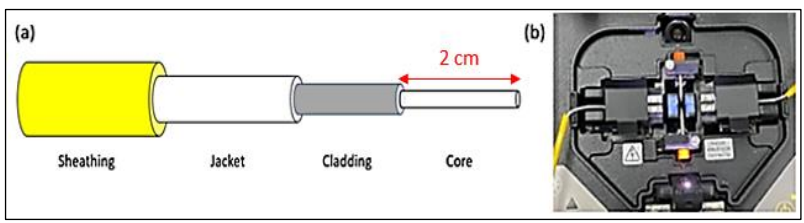


Figure 1: (a) Standard configuration of fibre optic probe (single core) used in this work and (b) the splicer was used to connect both ends of the core cable after being coated with sensing materials

## Characterization of AgNS, GO and GO-AgNS

The synthesized AgNS, GO, and GO-AgNS samples were characterized using UV-Vis spectroscopy (JASCO, v-670 UV-VIS-NIR spectrophotometer) to analyze their absorption spectra. UV-Vis spectroscopy scans were conducted using a quartz cuvette by diluting 30 µL of the sensing material solution with 2970 µL of deionized water. For morphological analysis of AgNS, transmission electron microscopy (TEM) (Philips CM12 Version 3.2) and field emission scanning electron microscopy (FESEM) (Hitachi SU3500) analyses were performed, and the length of AgNS was measured using ImageJ software. Meanwhile, the morphological and elemental analysis of synthesized GO and GO-AgNS was characterized using scanning electron microscopy (SEM) and

energy dispersive X-ray spectroscopy (EDX), with samples prepared on glass slides.

The coated probes (the sensing platform) underwent detailed examination using SEM to assess the optical quality of the surface and the quality of the coated layer. Cracks in the coating typically indicate improper conditions during synthesis and deposition. Conversely, a crack-free coating demonstrates mechanical strength equal to or greater than that of the underlying optical fibre [23]. SEM images captured were further analyzed for thickness measurements using ImageJ software. EDX analysis was performed as well to confirm the elemental composition of the coating layers on the surface of the coated probe.

## Signal performance of fibre optics sensors

The coated fibre optics (AgNS, GO, or GO-AgNS at various ratios) that have spliced were then ready for characterization on signal performance using the setup as shown in Figure 2. In this setup, the laser power supply (1064 nm, SDL-1064-500M6 6) was connected to the laser light source (wavelength 785 nm, SDL-785-LM-500M66) to provide light through the fibre optics cable. The fibre optics coated with the sensing materials (labelled as sensing platform in Figure 2) were then connected with a laser light source and spectrometer (Ocean Optics, HR400CG-UV-NIR).

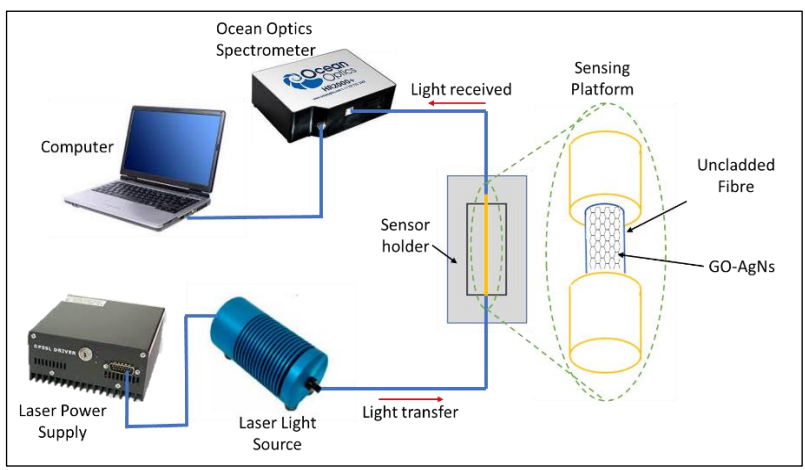


Figure 2: Experimental setup for signal performance using a fibre optic sensor with the red circle showing the sensing region

The spectrometer was then connected to a computer to detect the optical signal from the setup. The optical signal generated from each sensing material was then recorded (using Overture software) and analyzed in Excel software.

To determine the strongest coating material for the sensor platform, it is important to identify the optimal thickness of the sensing material coated onto the probe. This can be achieved by comparing the collected light intensity, recorded as the signal, for different coating thicknesses.

## Results and Discussion

### Characterization of AgNS

By conducting UV-Vis analysis on AgNS, the LSPR performances can be studied by running absorbances performance on it. Based on the result shown in Figure 3, the trend showed that the maximum peak of the spectrum was red-shifted (372 nm for Sample L, followed by 376 nm for Sample M, 390 nm for Sample N, and 392 nm for Sample O) as the concentration of hydroxylamine decreased. As the wavelength of the spectrum correlated with the size and shape of the NPs [21], this may indicate that the star-spike of AgNS expanded as more new nucleation was discarded with a limited amount of reducing agent presented. Here, hydroxylamine was used as a reducing agent in which the silver ion ($Ag^{+}$) was reduced to metallic silver ($Ag^{0}$) by donating electrons to reduce it causing the silver atom to aggregate and grow on the surface of the seed particle [17], eventually forming a nanostar structure.

In line with the findings of [24], the lower component observed in the range of ~360 nm - 380 nm in the UV-Vis spectra can be attributed to the quadrupolar plasmon resonance of the nanostar's core. Additionally, the presence of the ~415 nm - 420 nm component could be associated with transversal resonances of the tips or residual quasi-spherical nanoparticles. The dipolar plasmon resonances of nanostars with a diameter of 400 nm are expected to appear in the range of 600 nm - 700 nm for Ag, as indicated by single nanostar analysis using an enhanced dark-field technique [25]. However, the absence of clear resonances at these wavelengths for Samples L, M, and N can be attributed to two possible reasons. Firstly, the resulting nanoparticles' morphology may be relatively heterogeneous [26]. Secondly, significant aggregation of nanoparticles might occur leading to larger aggregates, which could explain the observed increase in extinction at higher wavelengths in these samples [27].

Sample O exhibits the highest peak intensity and greater morphological uniformity compared to the other AgNS samples. The observed low wavelength band at 363 nm - 370 nm corresponds to quadrupolar plasmon resonances, while the second maximum peak observed at 680 nm - 750 nm is associated with dipolar plasmon modes, consistent with previous findings [25] where single nanostars were successfully formed. The presence of branches in the star-shaped nanoparticles creates localized electromagnetic field enhancements known as "hot spots," enabling strong light interaction. Thus, the size and number of branches in AgNS play a crucial role in determining

the intensity of light interaction. Moreover, a high absorbance within the desired wavelength range, coupled with a narrow peak width, indicates improved optical properties and strong plasmonic resonances. Accordingly, Figure 3 demonstrates an increase in the peak intensity (absorbance) of the UV-Vis spectroscopy for Sample O, indicating a stronger light interaction compared to the other samples. The peak intensity of all AgNS samples was reassessed after 3 months, and the results remained consistent, demonstrating their long-term stability in fibre sensing.

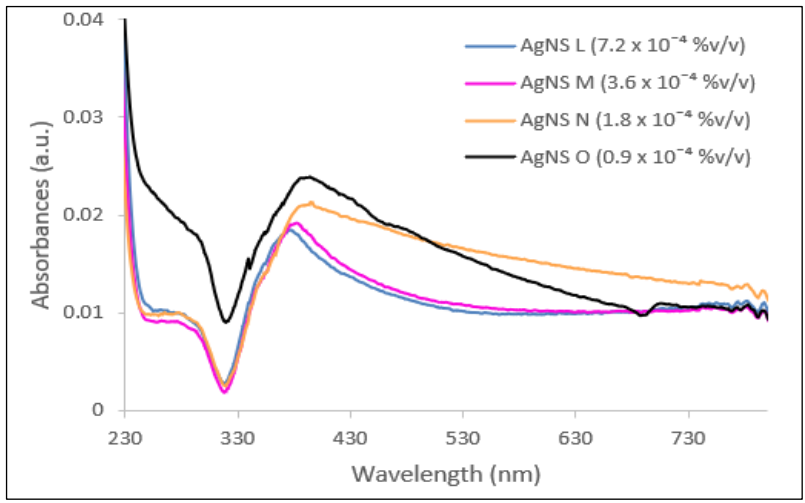


Figure 3: UV-Vis on AgNS samples synthesized using various concentrations of hydroxylamine

Figures 4 and 5 present the morphological analysis of AgNS samples (L, M, N, and O) using TEM and FESEM, respectively. The TEM images allowed for the measurement of the star-spike length, yielding values of 198.75 ± 69.03 nm for Sample L, 166.58 ± 77.04 nm for Sample M, 313.26 ± 66.26 nm for Sample N, and 352.62 ± 59.72 nm for Sample O. Figure 4 reveals a distinct change in the structure of AgNS as the concentration of hydroxylamine decreases. Notably, a reduction in hydroxylamine concentration leads to the formation of star-shaped structures with longer spikes. The morphological variations are clear in Figure 4(a) and Figure 5(a) of Sample L, where a lesser number of star-shaped structures and more irregular shapes, consisting of a mixture of round and short spikes (choral-like), were observed. This observation can be attributed to the fact that higher concentrations of the reducing agent promote increased nucleation, resulting in a reduced formation of star-shaped structures.

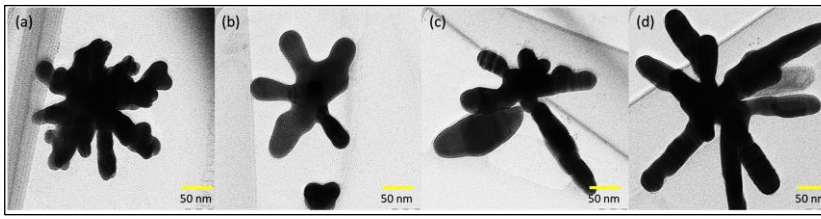


Figure 4: TEM images of AgNS of; (a) L, (b) M, (c) N, and (d) O samples

Comparing Samples M and N, it is apparent that the branch length of Sample N is longer than that of Sample M, indicating that Sample N offers a larger surface area for light interaction. This finding aligns with the analysis of the UV-Vis spectrum presented in Figure 3, where an increase in peak intensity is observed as the branch length of the star-shaped structures increases. The shapes of the star structures in Sample O are found to be more consistent, with the longest branch lengths compared to sample N. The FESEM analysis, as depicted in Figure 5, provides further insights into the morphological characteristics, including the distribution of nanoparticles, and allows for an assessment of overall uniformity and aggregation behaviour, which may relate to the absorption peak observed in the UV-Vis spectrum.

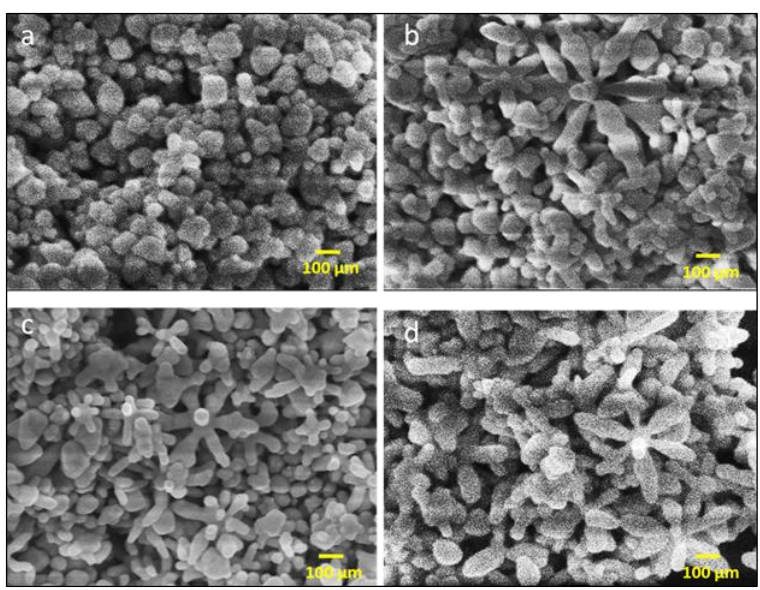


Figure 5: FESEM images of AgNS; sample of (a) L, (b) M, (c) N, and (d) O

It can be observed that Sample O shows a higher abundance of star-shaped particles compared to other samples. Therefore, due to its superior morphological uniformity in terms of star shape compared to the other samples, AgNS from Sample O was selected for further mixing with GO. The consistent and well-defined star shape observed in Sample O makes it an ideal choice for achieving a homogeneous and stable GO-AgNS composite.

## Characterization of GO-AgNS

Figure 6 shows UV-Vis results on GO, AgNS (sample O), and GO-AgNS at various mixing ratios. The result shows that the absorption peak of GO is observed at 233 nm, which agrees with the previous research [28] result indicating that the GO was successfully synthesized as exhibits $\pi$- $\pi$* transition of the C-C aromatic bond. By embedding together, the GO and the AgNS, the peak intensity of the UV-Vis spectrum for GO-AgNS is seen to increase compared to AgNS only. When the AgNS is embedded with GO, the effect of plasmon coupling occurs where the optical resonance of nanoparticles is tuned [29]. The effect of plasmon coupling happens due to the surface area of GO-AgNS increasing compared to AgNS only allowing high interaction with UV light. Thus, the peak intensity UV spectrum of GO-AgNS is higher than AgNS only.

To investigate the effect of the ratio of mixing GO-AgNS (1:5, 1:10, 1:15, and 1:20) on the UV-Vis spectrum, Figure 6 was analyzed. The aim was to determine if a higher amount of AgNS mixed with the same amount of GO would result in a higher peak intensity in the UV spectrum. However, contrary to the hypothesis, the results show that as the amount of AgNS increases relative to GO, the peak intensity of the UV-Vis spectrum decreases. The observed trend can be explained by considering the properties of GO and AgNS. GO exhibits higher absorption intensity compared to AgNS, and when GO is mixed with AgNS, there is a limit to how much AgNS can be effectively embedded within the GO structure. Therefore, when the ratio of AgNS to GO is increased, a larger amount of AgNS remains unembedded, leading to a reduction in the concentration of AgNS available for absorption. Consequently, the peak intensity of the UV spectrum decreases as a result.

Among the different mixing ratios, the GO-AgNS mixture with a ratio of 1:5 shows a higher peak UV intensity compared to the other ratios. This can be attributed to the optimal balance achieved between the amount of AgNS embedded within GO and the remaining unembedded AgNS. As the amount of AgNS further increases in the other ratios, the excess AgNS that does not embed within the GO matrix reduces the overall concentration of AgNS, resulting in a decrease in peak intensity.

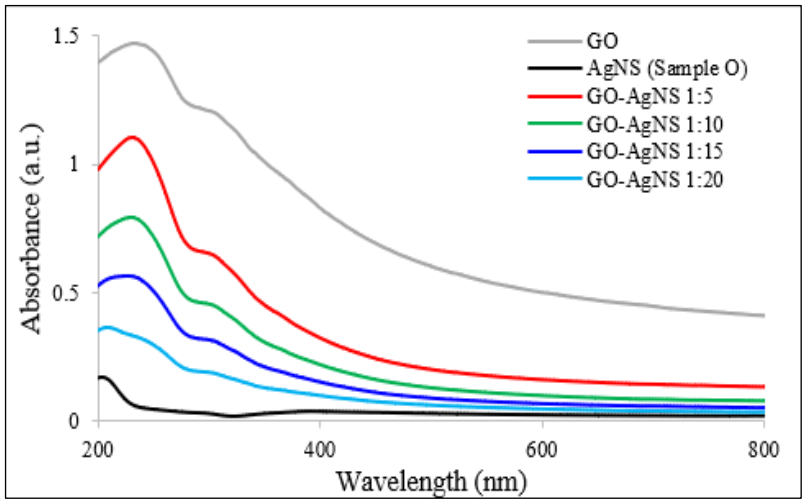


Figure 6: UV-Vis result of AgNS, GO, and GO-AgNS at various mixing ratios

EDX analysis was conducted to identify the elements and confirm the content of each sample. The result shows that the elements of silver (Ag), carbon (C), and oxygen (O) were detected in the scanning result as summarized in Table 2. The result indicates that the presence of silver increases as the ratio of AgNS in GO-AgNS increases. At the same time, the presence of carbon decreases indicating the amount of GO available for AgNS to inhibit decreases as well.

Table 2: EDX analysis on AgNS, GO, and GO-AgNS at various mixing ratios

| **Element (*at.*%)** | **AgNS** | **GO** | **GO-AgNS 1:5** | **GO-AgNS 1:10** | **GO-AgNS 1:15** | **GO-AgNS 1:20** |
|---|---|---|---|---|---|---|
| Carbon, C | 0 | 53.2 | 34.0 | 32.1 | 30.5 | 28.8 |
| Oxygen, O | 91.2 | 46.8 | 63.3 | 64.4 | 65.2 | 65.5 |
| Silver, Ag | 8.8 | 0 | 2.4 | 3.5 | 4.3 | 5.7 |

In order to further investigate the GO-AgNS mixtures with different ratios (1:5, 1:10, 1:15, and 1:20), SEM imaging was performed on samples deposited on a glass slide, as shown in Figure 7. The SEM images provide insights into the morphology and structure of the GO-AgNS composites, as well as the individual GO and AgNS samples. Figure 7(a) reveals the crinkle feature of the GO structure, indicating a successful synthesis process involving

the exfoliation of graphite into multi-layered graphite followed by the oxidation process that recombines and restructures a few layers with the assistance of an oxygen component, resulting in the formation of GO [19]. Analyzing the SEM images of GO-AgNS with different ratios (Figures 7(b), 7(c), 7(d), and 7(e)), it can be observed that the GO-AgNS composite with a ratio of 1:5 exhibits more white dots, representing the presence of AgNS particles on the GO structure. This finding supports the corresponding UV-Vis results (Figure 6) where the 1:5 ratio exhibited the highest absorption intensity among the GO-AgNS samples. The increased number of AgNS particles in the 1:5 ratio further confirms the higher concentration of AgNS embedded within the GO matrix, contributing to the higher absorption intensity observed in the UV-Vis spectrum.

On the other hand, as the amount of AgNS increases in the GO-AgNS mixtures, more excess AgNS is present, indicating a higher water content. Consequently, the concentration of AgNS becomes diluted, leading to a decrease in the number of white dots observed in the SEM image of the GO-AgNS composite with a ratio of 1:20. This dilution effect on AgNS concentration provides another explanation for the observed decrease in the peak intensity of the UV-Vis spectrum as more AgNS is mixed with GO.

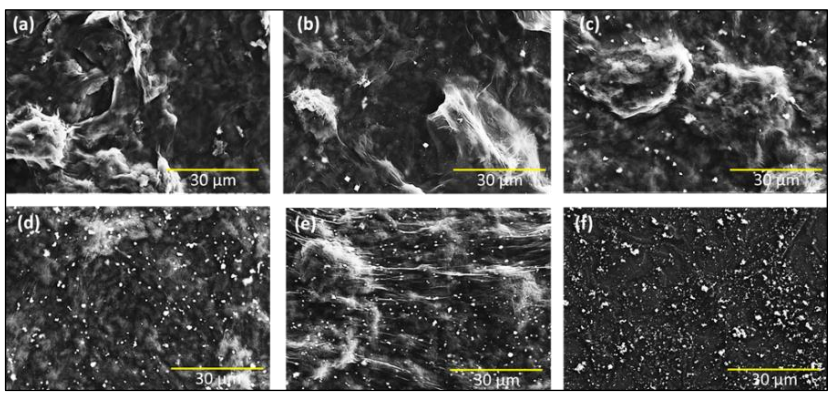


Figure 7: SEM images of (a) GO, GO-AgNS at a ratio of; (b) 1:20, (c) 1:15, (d) 1:10, and (e) 1:5 and (f) AgNS (Sample O)

## Characterization of fibre optics embedded sensing materials (AgNS, GO and GO-AgNS)

Figure 8 presents SEM images of the successfully embedded fibre optic sensor probes coated with AgNS, GO and GO-AgNS at their respective ratios. Analysis of these images allowed for the measurement of the average thickness of the coated fibre optics. The results show an average thickness of 122 ± 1 µm for AgNS, 123 ± 0.3 µm for GO, 123 ± 0.7 µm for GO-AgNS (ratio 1:5), 124

± 1 µm for GO-AgNS (ratio 1:10), 123 ± 1 µm for GO-AgNS (ratio 1:15), and 122 ± 0.8 µm for GO-AgNS (ratio 1:20).

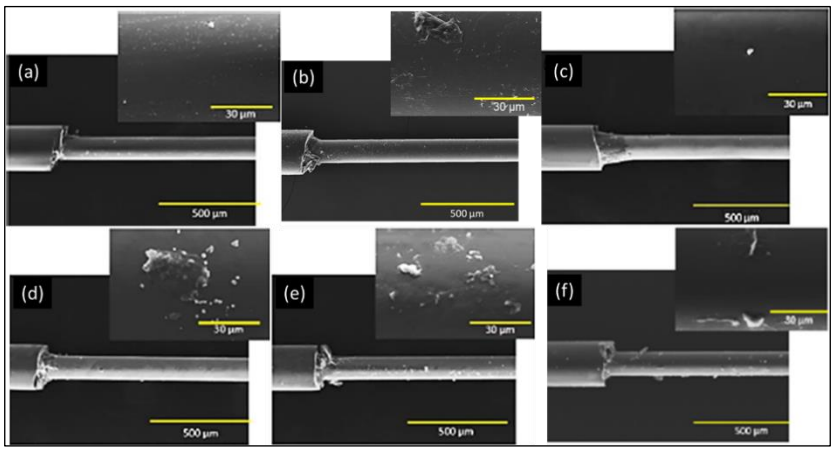


Figure 8: SEM images of the sensing platform coated with; (a) AgNS, (b) GO, and GO-AgNS at a ratio of (c) 1:5, (d) 1:10, (e) 1:15, and (f) 1:20

When the volume ratio of AgNS relative to GO is increased, more GO-AgNS deposits onto the surface, resulting in an increased thickness of the core layer. However, at the GO-AgNS ratio of 1:15, the thickness begins to decrease. This can be attributed to the presence of excess silver that did not embed within the GO matrix. Furthermore, as the water content increases in the colloidal AgNS at higher volumes, the concentration of AgNS becomes less concentrated, as indicated by the absorbance values in Figure 6. Consequently, this leads to a decrease in the amount of AgNS deposited during the coating process. Subsequently, the overall thickness of the coated fibre optics is reduced. Despite that, the fibre optics depicted in Figure 8 exhibit a smooth coating of AgNS on the bare fibre optics without any visible signs of cracking. This remains true even when embedding different ratios of AgNS, GO, and GO-AgNS. This observation suggests that the coating layer of the sensing materials possesses notable mechanical strength [29]. Consequently, it is expected that this mechanically strong coating will enable the provision of a robust optical signal to the sensor.

EDX testing was performed to analyze the elemental composition by scanning the surface of the fibre optic probe. This analysis facilitated the identification of the elements present and verified the successful coating of each sensing material onto the core of the probe, as summarized in Table 3. The presence of silica (Si) in the scanning results is attributed to the core material of the probe, which is composed of silica. Despite the coating layer

being only a few nanometers thick, the Si element can still be detected by the EDX probe. However, as the thickness of the coating layer increases, the presence of detected Si gradually decreases. Here, the detection of C on the AgNS-coated probe can be attributed to the residue of the unclad layer of the probe as no C element was detected on the EDX result of the AgNS sample presented in Table 2. Furthermore, with the addition of GO to the AgNS samples, the carbon content increases, indicating the successful loading of AgNS onto the GO structures, which in turn coat the fibre optic probe.

Table 3: EDX analysis on fibre optics coated with AgNS, GO, and GO-AgNS at various ratios

| **Element (*at.*%)** | **AgNS** | **GO** | **GO-AgNS 1:5** | **GO-AgNS 1:10** | **GO-AgNS 1:15** | **GO-AgNS 1:20** |
|---|---|---|---|---|---|---|
| Carbon, C | 7.0 | 21.4 | 7.4 | 8.3 | 9.92 | 12.1 |
| Oxygen, O | 58.9 | 42.3 | 55.8 | 55.5 | 55.08 | 54.2 |
| Silver, Ag | 0.1 | 0 | 0.1 | 0.1 | 0.02 | 0.1 |
| Silica, Si | 36.0 | 36.3 | 36.7 | 36.1 | 34.98 | 33.6 |

## Evaluation of signal performance of fibre optics sensors

The coated fibre optics, incorporating AgNS, GO, and GO-AgNS at different ratios, were connected to Ocean optics spectrometers to obtain signal readings. Figure 9 displays the results obtained from the spectrometer. It can be observed that the signal generated from AgNS is significantly higher than that generated from GO. This can be attributed to the smaller size and higher sensitivity offered by the nanoscale dimensions of AgNS compared to GO, even though the thickness of the AgNS coated is lowered than GO-coated probe. Additionally, the star-shaped structure of AgNS also contributes to the higher signals, consistent with findings from [25]. However, the signals generated by the individual sensing materials are relatively low compared to the signals generated by the composite material system (GO-AgNS). This suggests that the composite structure of sensing materials outperforms the individual components, as evidenced by the signals represented by the AgNS (black line) and GO (grey line) samples in Figure 9.

Among the different ratios tested, the sensing platform coated with GO-AgNS at a volume ratio of 1:5 exhibits the highest signal, surpassing the other samples. The signal improvement is approximately 218% compared to the signal generated by GO alone and 174% compared to the AgNS signal. This enhanced performance can be attributed to the ability of GO to coat a greater amount of sensing material on the fibre optic core while retaining the AgNS within its structure, thereby preventing light leakage. Furthermore, the presence of AgNS in the GO-AgNS composite further enhances the signal. However, as the volume ratio of AgNS solution to GO increases (green, blue,

and yellow lines in Figure 9), the signal performance decreases. This is due to the decreased total volume concentration, which reduces the likelihood of GO-AgNS particles being effectively coated onto the probe, as supported by previous findings from UV-Vis, SEM, and EDX analyses. Hence, the optimum sensing material is found to be the composite GO-AgNS at a volume ratio of 1:5. This composite can serve as an effective sensing platform, which can be further utilized in conjunction with biomolecules or other target materials to improve the signal of fibre-optic sensors.

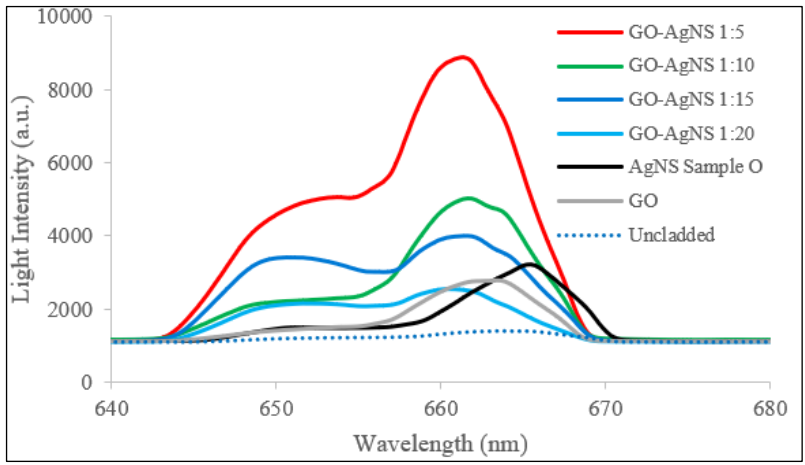


Figure 9: Sensor signals generated when embedded with different sensing materials including AgNS, GO, and GO-AgNS at volume ratios of 1:5, 1:10, 1:15, and 1:20

The mechanism of the sensing platform can be explained through TIR occurrences in the core of the fibre. As the light passed through the core, a portion of the light ray was reflected. Another portion that fails to reflect will interact with the cladding region, leading to a gradual reduction in light intensity exponentially as it moves away from the interface. These incidents will form an evanescent field within the cladding region. The light within the cladding region is reflected at the top surface of the cladding, redirecting it back into the core region, thus enhancing the overall light output. The AgNS and GO-AgNS that replace the cladding layer will amplify the light output through the absorption and excitation of light in the AgNS of the cladding region. This phenomenon is called LSPR and the amplification of light will depend on the size, shape, and composition of nanoparticles. However, due to the agglomeration tendency of AgNS, light amplification becomes unstable, resulting in unreliable signal detection. Therefore, the presence of GO prevents

AgNS agglomeration which will assist in stabilizing the signal detection, thus significantly amplifying the signal of the sensors.

## Conclusions

In conclusion, the experimental data obtained reveal that the AgNS with the longest star-spike measured at 352.62 ± 59.72 nm (Sample O) was successfully synthesized using specific concentrations: 0.05 M of NaOH, 0.9 x $10^{-4}$ %v/v of hydroxylamine, 8 x $10^{-4}$ M of $AgNO_3$, and 0.045 M of sodium citrate tribasic dehydrate. Furthermore, the successful synthesis of GO was confirmed through UV-Vis, SEM, and EDX analysis. The optical properties of GO-AgNS composites were investigated by fabricating different ratios. Among them, the GO-AgNS composite with a ratio of 1:5 exhibited the highest optical absorbance. Moreover, this composite displayed a more uniform structure, rendering it suitable for utilization in the sensing platform of fibre optics. Signal analysis was conducted to evaluate the performance of the GO-AgNS composite. Remarkably, when the optical fibre was coated with GO-AgNS at a volume ratio of 1:5, a significant improvement in sensing ability was observed. Specifically, the signal enhancement reached up to 218% compared to the GO-coated probe signal and 174% compared to the AgNS-coated probe signal. These findings highlight the potential of the GO-AgNS composite structures to enhance the sensitivity of fibre optic sensors. Consequently, these advancements hold great promise for the development of super-sensitive devices and open up opportunities for a wide range of applications, including advanced sensing, biomedical applications and environmental monitoring. It is highly recommended to apply the surface treatment method on the unclad fibre optics before embedding them with sensing materials. This process brings about significant improvements in the adhesion and strength of the sensing materials, which becomes especially crucial when considering their utilization in microfluidic-based biosensors. Preventing cracking or detachment is of utmost importance in such systems. The enhanced adhesion and strength of the sensing materials greatly contribute to a more dependable and resilient performance in these respective fields.

## Contributions of Authors

The authors confirm the equal contribution in each part of this work. All authors reviewed and approved the final version of this work. Azib: Data curation, Writing – original draft, formatting. Dr. Siti Rabizah Makhsin: Validation, Supervision, Writing – review and editing, formatting, submission. Ir Ts Dr Rozina Abdul Rani: Co-supervisor, review. Dr Beenish: Review.

## Funding

This work is financially supported by the Global Research Grant, UiTM (600-RMC5/3/GRR(008/2020)), and GIP grant UiTM (600-RMCGIP5/3(106 /2022).

## Conflict of Interests

All authors declare that they have no conflicts of interest.

## Acknowledgment

The authors would like to thank the Micro-Nano Electro Mechanical System Lab (MiNEMS), School of Mechanical Engineering, UiTM, College of Engineering, UiTM Shah Alam, and Vector Control Research Units, USM for their technical support.

## References

[1] A. K. Singh, S. Mittal, M. Das, A. Saharia, and M. Tiwari, "Optical biosensors: A decade in review," *Alexandria Engineering Journal*, vol. 67, pp. 673–691, 2023. doi: 10.1016/J.AEJ.2022.12.040

[2] S. Addanki, I. S. Amiri, and P. Yupapin, "Review of optical fibers-introduction and applications in fiber lasers", *Results in Physics*, vol. 10, pp. 743–750, 2018. doi: 10.1016/J.RINP.2018.07.028

[3] W. S. Jiang, W. Xin, S. Xuan, S. N. Chen, X. G. Gao, Z. B. Liu, and J. G. Tian, "Reduced graphene oxide-based optical sensor for detecting specific protein", *Sensors Actuators B: Chemical*, vol. 249, pp. 142–148, 2017. doi: 10.1016/J.SNB.2017.03.175

[4] O. Bratash, A. Buhot, L. Leroy, and E. Engel, "Optical fiber biosensors toward in vivo detection.", *Biosensors and Bioelectronics*, vol. 251, pp. 1-19, 2024. doi: 10.1016/J.BIOS.2024.116088

[5] M. A. Butt, G. S. Voronkov, E. P. Grakhova, R. V. Kutluyarov, N. L. Kazanskiy, and S. N. Khonina, "Environmental monitoring: A comprehensive review on optical waveguide and fiber-based sensors", *Biosensors*, vol. 12, no. 11, pp. 1-31, 2022. doi: 10.3390/BIOS12111038

[6] V. Nandre, Y. Jadhav, D. K. Das, R. Ahire, S. Ghosh, S. Jadkar, K. Kodam, and S. Waghmode, "Nanomaterials for sensors: Synthesis and applications", *Advanced Nanomaterials for Point of Care Diagnosis and Therapy*, pp. 477–492, 2022. doi: 10.1016/B978-0-323-85725-3.00011-

8

[7] A. A. Polokhin, Y. P. Shaman, P. A. Itrin, I. S. Panyaev, A. A. Sysa, S. V. Selishchev, E. P. Kitsyuk, A. A. Pavlov, and A. Y. Gerasimenko, "Tapered optical fiber sensor coated with single-walled carbon nanotubes for dye sensing application", *Micromachines*, vol. 14, no. 3, pp. 1-11, 2023. doi: 10.3390/MI14030579

[8] A. Rashid, M. Haque, S. M. M. Islam, and K. M. R. Uddin Labib, "Nanotechnology-enhanced fiber-reinforced polymer composites: Recent advancements on processing techniques and applications", *Heliyon*, vol. 10, no. 2, pp. 1-29, 2024. doi: 10.1016/J.HELIYON.2024.E24692

[9] S. Lee, H. Song, H. Ahn, S. Kim, J. ryul Choi, and K. Kim, "Fiber-optic localized surface plasmon resonance sensors based on nanomaterials", *Sensors*, vol. 21, no. 3, pp. 1-22, 2021. doi: 10.3390/S21030819

[10] J. A. Dionne, "Lights, nano, action! New plasmonic materials and methods to probe nanoscale phenomena," *MRS Bulletin*, vol. 40, no. 3, pp. 264–270, 2015. doi: 10.1557/MRS.2015.31/FIGURES/4

[11] F. Sadeghfar and M. Ghaedi, "Photocatalytic treatment of pollutants in aqueous media," *Interface Science and Technology*, vol. 32, pp. 725–759, 2021. doi: 10.1016/B978-0-12-818806-4.00011-5

[12] B. Sepúlveda, P. C. Angelomé, L. M. Lechuga, and L. M. Liz-Marzán, "LSPR-based nanobiosensors", *Nano Today*, vol. 4, no. 3, pp. 244–251, 2009. doi: 10.1016/J.NANTOD.2009.04.001

[13] R. Ghosh Chaudhuri and S. Paria, "Core/shell nanoparticles: Classes, properties, synthesis mechanisms, characterization, and applications", *Chemical Reviews*, vol. 112, no. 4, pp. 2373–2433, 2012 doi: 10.1021/CR100449N/ASSET/IMAGES/CR-2010-00449N_M017.GIF

[14] K. Malecka, B. Kaur, D. A. Cristaldi, C. S. Clay, I. Mames, H. Radecka, J. Radecki, and Eugen Stulz, "Silver or gold? A comparison of nanoparticle modified electrochemical genosensors based on cobalt porphyrin-DNA", *Bioelectrochemistry*, vol. 138, pp. 1-8, 2021. doi: 10.1016/J.BIOELECHEM.2020.107723

[15] A. M. Leach, M. McDowell, and K. Gall, "Deformation of top-down and bottom-up silver nanowires", *Advanced Functional Materials*, vol. 17, no. 1, pp. 43-53, 2007. doi: 10.1002/ADFM.200600735

[16] A. Loiseau, V. Asila, G. Boitel-Aullen, M. Lam, M. Salmain, and S. Boujday, "Silver-based plasmonic nanoparticles for and their use in biosensing", *Biosensors*, vol. 9, no. 2, pp. 1-39, 2019. doi: 10.3390/bios9020078

[17] A. Garcia-Leis, J. V. Garcia-Ramos, and S. Sanchez-Cortes, "Silver nanostars with high SERS performance," *The Journal of Physical Chemistry C*, vol. 117, no. 15, pp. 7791-7795, 2013. doi: 10.1021/jp401737y

[18] M. Kaur, H. Kaur, and D. Kukkar, "Synthesis and characterization of

graphene oxide using modified Hummer's method," *AIP Conference Proceedings*, vol. 1953, no. 1, pp. 1-5, 2018. doi: 10.1063/1.5032515/817677

[19] S. Mukherjee, A. Mukherjee, Z. Bytesnikova, A. M. Ashrafi, L. Richtera, and V. Adam, "2D graphene-based advanced nanoarchitectonics for electrochemical biosensors: Applications in cancer biomarker detection", *Biosensors and Bioelectronics*, vol. 250, pp. 1-19, 2024. doi: 10.1016/J.BIOS.2024.116050

[20] M. R. Sahudin, M. Zourob, M. H. Noor Akashah, R. Abdul Rani, and S. R. Makhsin, "Physical properties of graphene", *Journal of Mechanical Engineering*, vol. 12, no. 1, pp. 225-267, 2023. doi: 10.24191/jmeche.v12i1.24649

[21] D. B. Thinh, D. N. Minh, L. T. Tai, N. Duy, N. T. Tinh, L. M. Huong, D. Tran, Q. Thi, T. Huong, N. Thanh, H. Nam, D. Thi, D. T. Y. Oanh, P. T. Mai, H. H. Nguyen, and T. N. N. Kim, "A review of silver-dopped graphene oxide nanocomposite: Synthesis and multifunctional applications," *Vietnam Journal of Chemistry*, vol. 60, no. 5, pp. 553–570, 2022. doi: 10.1002/VJCH.202200034

[22] A. H. Bin Roslan, S. R. B. Makhsin, R. A. Rani, K. A. Razak, and M. Zourob, "One-step synthesis of nanostar shaped silver nanoparticles and its optical stability," *IEEE International Conference on Semiconductor Electronics*, pp. 129–132, 2022. doi: 10.1109/ICSE56004.2022.9863200

[23] S. R. Makhsin, K. A. Razak, and R. Noordin, "Development of silver-coated gold nanoparticles and its conjugation for labeling on lateral flow immunoassay", *Advanced Materials Research*, vol. 1024, pp. 273–276, 2014. doi: 10.4028/WWW.SCIENTIFIC.NET/AMR.1024.273

[24] D. P. Sudas, V. A. Jitov, And P. I. Kuznetsov, "Various types of light guides for use in lossy mode resonance-based sensors", *Sensors*, vol. 23, no. 13, pp. 1-12, 2023. doi: 10.3390/S23136049

[25] A. Garcia-Leis, I. Rivera-Arreba, and S. Sanchez-Cortes, "Morphological tuning of plasmonic silver nanostars by controlling the nanoparticle growth mechanism: Application in the SERS detection of the amyloid marker Congo Red", *Colloids and Surfaces A: Physicochemical and Engineering Aspects*, vol. 535, pp. 49–60, 2017. doi: 10.1016/J.COLSURFA.2017.09.013

[26] M. K. Ha, K. H. Chung, and T. H. Yoon, "Heterogeneity in biodistribution and cytotoxicity of silver nanoparticles in pulmonary adenocarcinoma human cells", *Nanomaterials*, vol. 10, no. 1, pp. 1-13, 2019. doi: 10.3390/NANO10010036

[27] J. Piella, N. G. Bastús, and V. Puntes, "Modeling the optical responses of noble metal nanoparticles subjected to physicochemical transformations in physiological environments: Aggregation, dissolution and oxidation", *Zeitschrift fur Physikalische Chemie*, vol. 231, no. 1, pp. 33–50, 2017. doi: 10.1515/ZPCH-2016-0874/ASSET/GRAPHIC/J_ZPCH-2016-

0874_FIG_007.JPG

[28] S. Sunderrajan, L. R. Miranda, and G. Pennathur, "Improved stability and catalytic activity of graphene oxide/chitosan hybrid beads loaded with porcine liver esterase", *Preparative Biochemistry & Biotechnology*, vol. 48, no. 4, pp. 343–351, 2018. doi: 10.1080/10826068.2018.1446153

[29] P. K. Jain, X. Huang, I. H. El-Sayed, and M. A. El-Sayed, "Noble metals on the nanoscale: Optical and photothermal properties and some applications in imaging, sensing, biology, and medicine," *Accounts of Chemical Research*, vol. 41, no. 12, pp. 1578–1586, 2008. doi: 10.1021/AR7002804